Sensors & Actuators: A. Physical 373 (2024) 115445

Contents lists available at ScienceDirect

Sensors and Actuators: A. Physical

journal homepage: www.journals.elsevier.com/sensors-and-actuators-a-physical

Robustness of embedded fibre optic sensor mesh configurations for monitoring composite structures

James M. Gilbert *, Kaushal Bhavsar, Oleg V. Ivanov

School of Engineering, University of Hull, Hull HU6 7RX, UK

ARTICLE INFO

Keywords:
Fiber optic sensor
Fiber Bragg grating

ABSTRACT

Fibre optic sensors are attractive for monitoring of composite structures but the significant risk of damage to fibres where they enter the structure and within the structure itself can make their use unreliable. Mesh configurations of embedded fibre Bragg grating sensors with improved robustness are considered for monitoring composite structures. The configurations of single ended line, bidirectional line, loop, and a novel 2×2 mesh are analysed using a probabilistic model of the sensor system robustness. Numerical evaluation of these configurations has shown that the 2×2 mesh configuration provides the greatest robustness of all of the configurations across all inlet port failure probabilities. The probability of a sensor becoming isolated in a 2×2 mesh is approximately 3 times lower than for the bidirectional line configuration. Using a new matrix approach, the 2×2 mesh configuration is analysed in terms of disaggregation of individual sensor spectra for both fault free and faulty conditions. Simulation and experimental evaluation have demonstrated that successful recovery of individual grating spectra is possible with small spurious signals.

1. Introduction

Fibre optic sensors have many benefits for monitoring the manufacture and operation of large composite structures such as wind turbine blades [1,2], aircraft fuselages [3], automobile, airspace, and others. Such sensors can be useful at different stages of lifespan of composite components for infusion control during fabrication, structural health monitoring, or damage diagnostics [4,5]. Although fibres may be attached to structures post-manufacture for operational monitoring, this surface mounting makes the sensors vulnerable to damage and so embedded sensors may be advantageous. Monitoring of the manufacturing process implies that sensors are imbedded within the structure. Embedded sensors have advantages in that they provide more flexibility in terms of the placement of sensors within the structure and sensors are protected from superficial damage. However, the nature of the composite structure and the manufacturing process introduce specific restrictions on the embedded sensor systems and results in specific fibre damage mechanisms, particularly associated with the points where fibres enter the structure.

An attractive feature of fibre optic sensors, particularly fibre Bragg gratings (FBGs), is the ability to fabricate multiple sensors into a single fibre and interrogate individual sensors using time or wavelength division multiplexing [6]. However, this approach means that if the single fibre becomes damaged then some or all of the sensors may become permanently isolated.

In response to the restrictions and damage mechanisms found in composite structure monitoring, a number of novel fibre connection configurations have been proposed with the aim of ensuring continued operation in the presence of imperfections or damage [7–10]. This paper presents the analysis of the robustness of alternative fibre configurations to the damage mechanisms found in composite manufacturing processes.

The typical Vacuum Assisted Resin Transfer Moulding manufacturing process for a composite structure involves laying up multiple sheets of glass/carbon fibre reinforcement within a mould and then injecting a liquid resin, driven by either positive pressure at the inlet, vacuum applied to the outlet or some combination of these [11]. The polymer resin then cures (often accelerated by the application of external heating), forming a solid composite. Ideally, the resin completely impregnates the reinforcement, filling all of the voids between fibres. However, in some cases the infusion is not complete and ‘dry spots’ remain in the structure. These areas may have to be reworked, involving removal of the partially impregnated reinforcement and replacement with new reinforcement and resin.

* Corresponding author.
E-mail address: j.m.gilbert@hull.ac.uk (J.M. Gilbert).

https://doi.org/10.1016/j.sna.2024.115445
Received 29 September 2023; Received in revised form 1 May 2024; Accepted 4 May 2024
Available online 9 May 2024
0924-4247/

The point at which the optical fibre enters the composite structure is particularly susceptible to damage during manufacture while fibres may also be damaged during the layup, infusion and curing processes. In addition, if it is necessary to 'rework' sections of a composite structure, the optical fibres in that region would be removed along with the partially impregnated reinforcement. Damage may also occur during operation, once again at the fibre entry point due to mishandling and in the bulk of the structure if it is damaged due to impacts or fatigue.

Given the susceptibility to damage of fibres at points where they enter the structure, it is desirable to optimise the number of entry points. Thus, it may be preferable to embed any coupling or switching elements within the composite structure rather than place them externally. In addition, since composite structures such as wind turbine blades and aircraft wings must be immune to lightning strikes, it is usually necessary to eliminate any electrical components within the structure. Hence, for this paper, it will be assumed that only passive components are embedded within the structure. This is in contrast to authors who propose the use of electrically active Remote Nodes [12,13], which would imply embedding electrical components within the structure. In addition, it will be assumed that components embedded within the structure cannot be accessed or replaced after manufacture.

2. Fibre optic sensor connections

In a conventional multi-point FBG sensing system, a number of FBGs with distinct Bragg wavelengths would be fabricated in a single fibre which would be interrogated from one end through reflection, as shown in Fig. 1, where fibres F_1 to F_n connect sensors S_1 to S_n, light from the light source is coupled into the fibre via the circulator and reflected light is coupled to the optical spectrum analyser (OSA).

Due to the limited optical bandwidth of light source and OSA, the number of FBGs which can be individually interrogated is limited to typically around 10 and so, for larger area monitoring, an array of fibres may be adopted, as shown in Fig. 2 with optical switches used to interrogate each string successively. The configuration shown in Fig. 2 implies that FBGs are interrogated using transmission rather than reflection but a similar configuration could be used for interrogation through reflection.

The configurations shown in Fig. 1 and Fig. 2 are highly susceptible to damage. In the case of Fig. 1, damage at the fibre entry point would isolate all sensors, and damage within the body of the structure would make some or all of the sensors isolated, depending on the fault location. In the case of Fig. 2, working in transmission, damage to a string at either the entry or exit point, or within the body of the structure would result in all sensors in the string being isolated.

The lack of robustness of the conventional line configuration has been considered in the literature in the context of general engineering structures (rather than specifically for composites) and more robust configurations identified (see Zhang [14] for a qualitative review of selected configurations). However, some of these proposed configurations are not applicable in the context of composite structures (for instance because of the use of active Remote Nodes [12,13,15]) or are excessively complex (for instance the Bus Protection Network proposed by Urquhart [16]) and so a number of alternatives are proposed here. These include mesh structures shown conceptually in Fig. 3. These cells may be coupled together to give larger mesh structures, but it is not clear that this would be necessary in most circumstances.

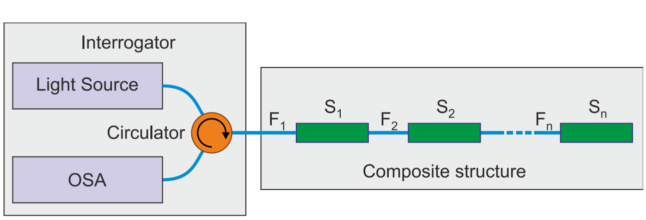

Fig. 1.. Line configuration of FBGs.

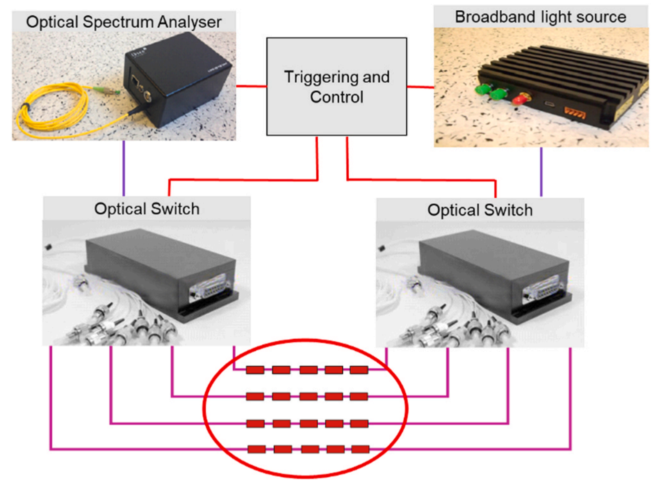

Fig. 2. Array configuration to increase number of FBG sensing points.

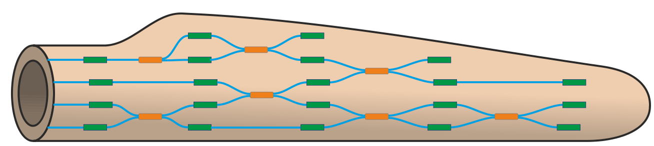

Fig. 3. Sensor mesh concept with coupled optical fibre sensors.

In the following sections a number of alternative fibre sensor configurations will be described, including ones proposed in the literature and a new mesh configuration. These will be evaluated in terms of their robustness to damage in the various fibre sections. In all cases. it will be assumed that damage to a fibre results in complete loss of optical connection at that point. In addition, it will be assumed that all sensors have a distinct Bragg wavelength and their reflection peaks do not overlap under the expected range of stimuli.

2.1. Single ended line configuration

The fibres and sensors in the conventional single ended line configuration are arranged along a single fibre and interrogated through reflection from one end, as shown in Fig. 4.

In this configuration a fault in the entry fibre F_1 will isolate all of the sensors from the interrogation system. A fault in fibre F_j will isolate all sensors S_i for $i \geq j$.

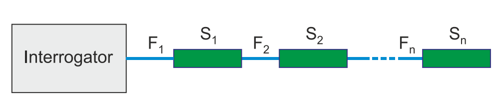

Fig. 4. Sensors in single ended line configuration of FBGs.

2.2. Bidirectional line configuration

In this configuration a string of sensors along a single fibre may be interrogated from either end, as illustrated in Fig. 5, using an optical switch to connect the interrogation system to each end of the line successively in a manner similar to that presented by Yeh [17].

In this configuration a single fault in one of the entry points F_1 or F_{n+1} or any of the intermediate fibres will not isolate any of the sensors. Sensors will only become isolated in the presence of two or more faults. In the case of faults in fibres F_j and F_k, the intermediate sensors S_i for $j \leq i \leq k$ will be isolated.

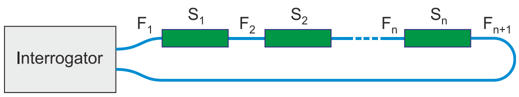

Fig. 5. Sensors in bidirectional line configuration of FBGs.

2.3. Loop configuration

The string of sensors may be looped back to form a loop configuration with a coupler connection as shown in Fig. 6, as proposed by Zhang [18,19]. In the form proposed, it is no clear that these configurations would give the desired output since transmitted and reflected signals would be combined in the coupler, resulting in all wavelengths being returned to the OSA ($T + R \cong 1$). However, the addition of an attenuator to the loop may enable successful operation. In the configuration shown in Fig. 6, the coupler may be placed outside of the structure or alternatively be embodied within the structure.

In these configurations a fault in F_0 will isolate all of the sensors. A single fault elsewhere in the loop will not isolate any sensors but sensors will only become isolated in the presence of two or more faults. In the case of faults in fibres F_j and F_k, the intermediate sensors S_i for $j \le i \le k$ will be isolated.

2.4. 2×2 mesh configuration

In order to increase the number of optical paths to a particular sensor, a coupler may be positioned within the mesh as shown in Fig. 7. This is a development of the embedded coupler configuration presented by Gillooly [20]. In this implementation the arms of the mesh are symmetric with $m = n/4$ sensors in each arm, although this is not necessarily the case. It should be noted that to simplify notation, the fibres leading into the coupler are numbered F_{c1} to F_{c4}.

In this configuration, the mesh may be interrogated in reflection from any of the 4 ports u_1 to u_4 using a 1×4 optical switch. Considering interrogation from port u_1, when all fibres are intact, sensors S_1 to S_m will be directly visible while S_{m+1} to S_{2m} and S_{2m+1} to S_{3m} are visible via the coupler, with the optical strength reduced by a factor of approximately $\frac{1}{4}$, assuming a 50:50 coupler is used. Similarly, each port allows sensors in 3 branches to be interrogated. Conversely, any sensor string can be interrogated from any one of 3 ports. This characteristic, along with the reduced number of fibres in each arm, leads to potentially improved robustness since there are fewer scenarios where sensors become isolated.

Sensors will only become isolated if two faults occur in a single arm of the mesh. In the case of faults in fibres F_j and F_k, the intermediate sensors S_i for $j \le i \le k-1$ will be isolated where j and k fall within a single arm of the mesh or, in the case of a fault in fibre j and in the fibre leading to the coupler, F_{cq}, sensors S_i for $j \le i \le mq$ will be isolated.

3. Probabilistic model of sensor system robustness

The level of robustness achievable with each of these configurations will depend on the probabilities of different fault types. Probabilistic models have been developed based on the method adopted by Zhang [18,21,22] and verified through numerical simulations. Zhang [18] presented results for single ended line and ring configurations, as well as star and bus configurations which are not considered here since they provide poorer robustness than the simpler configurations. Zhang did not consider the bidirectional line or the mesh configuration proposed here.

Let the probability of section i of the mesh being intact be denoted p_i. Where the fibre enters the structure the probability of the connection being intact will be denoted Inlet Probability P_I. Once within the body of the structure, the probability of impact damage or damage due to rework depends on the length of the fibre section considered (it is less likely that a fault will occur in a short section than a long section). The probability of damage may be different in different regions of the structure (for instance, rework may be more likely in some regions than others) but it will be assumed here that the probability of damage is uniform across the structure. The probability of a fault per unit length of fibre in the body of the structure will be denoted q. For a length of fibre, L_i within the body, the probability of no fault occurring may be calculated as $p_i = (1-q)^{L_i}$. It will be assumed that all links are of the same length, L, and hence the probability of a link fault is $P_L = (1-q)^L$.

It is assumed that all links external to the composite structure are intact (or could be replaced if damaged). The probability of a fault in a coupler embedded in the structure is denoted P_c. It will be assumed that damage results in complete loss of optical connection.

3.1. Single ended line configuration

For the single ended line topology shown in Fig. 4, the optical path involves one inlet port and a number of fibre links and so the probability of each link being intact is:

$$p_j = \begin{cases} P_I, \&j = 1 \\ P_L, \&j = 2 \ldots n \end{cases} \tag{1}$$

And the probability of l sensors being accessible, $P(l)$ is [18]:

$$P(l) = \begin{cases} 1 - p_1 \quad l = 0 \\ (1 - p_{l+1}) \prod_{j=1}^{l} p_j \quad l = 1, \quad 2, \quad \ldots n-1 \\ \prod_{j=1}^{n} p_j \quad l = n \end{cases} \tag{2}$$

So, the probability of all n sensors being accessible is

$$P_{\text{line}} = P(n) = \prod_{j=1}^{n} p_j = p_I p_L^n \tag{3}$$

3.2. Bidirectional line configuration

For the line configuration interrogated from either end, as shown in Fig. 5, the probability of each link being intact is:

$$p_j = \begin{cases} P_I, \&j = 1 \\ P_L, \&j = 2 \ldots n \\ P_I, \&j = n+1 \end{cases} \tag{4}$$

In this configuration, sensors only become isolated if two faults occur in difference sections of the fibre. The probability of fewer than 2 faults and hence all sensors being accessible is:

$$P(<2) = \left(1 + \sum_{t=1}^{n+1} \frac{1 - p_t}{p_t}\right) \prod_{j=1}^{n+1} p_j = [2p_L + (n - np_L - 1)p_I] p_I p_L^{n-2} \tag{5}$$

3.3. Loop configurations

Two versions of the configuration shown in Fig. 6 may be considered. If the coupler is placed outside of the composite structure then there are two inlet ports (dual inlet configuration). If the coupler is within the composite structure then there is only one inlet port (single inlet configuration). The link intact probabilities are:

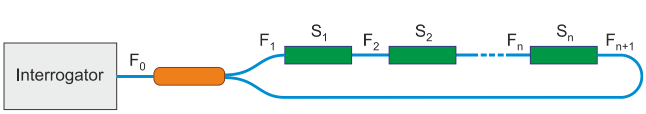

Fig. 6. Loop configuration with coupler.

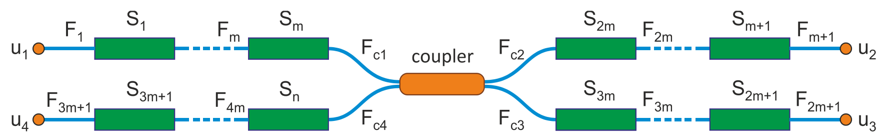

Fig. 7. 2×2 mesh configuration.

$$\text{Dual inlet}p_j = \begin{cases} 1, \&j = 0 \\ P_I, \&j = 1 \\ P_L, \&j = 2 \ldots n \\ P_I, \&j = n+1 \end{cases} \tag{6}$$

$$\text{Single inlet}p_j = \begin{cases} P_I, \&j = 0 \\ P_L, \&j = 1 \ldots n+1 \end{cases} \tag{7}$$

Note that for the dual inlet configuration, fibre F_0 is outside of the composite structure and so is assumed to be immune to damage or to be replaceable. Under this assumption, the configuration is the same as the line configuration with bidirectional interrogation and so Eq. (5) applies. In the case of the single inlet, link F_0 has a finite probability of failure and so the probability of all links being intact or one fibre apart from F_0 being broken is given by Eq. 8 (not the change in index in the product term):

$$\begin{aligned} P(<2) &= \left(1 + \sum_{t=1}^{n+1} \frac{1-p_t}{p_t}\right) \prod_{j=0}^{n+1} p_j \\ &= \begin{cases} [2p_L + (n - np_L - 1)p_I]p_I p_L^{n-2} \text{ Single inlet} \\ (1 + n - np_L)p_I p_L^n \text{ Dual inlet} \end{cases} \end{aligned} \tag{8}$$

3.4. 2×2 mesh configuration

For the mesh configuration each arm will be treated separately, with a single arm made up of $m = \frac{n}{4}$ sensors having the topology shown in Fig. 8.

Assuming no faults occur in the coupler, the link probabilities in the first arm are:

$$p_j = \begin{cases} P_I, \&j = 1 \\ P_L, \&j = 2 \ldots \frac{n}{4} \end{cases} \tag{9}$$

With interrogation from either end, on the left through the inlet, on the right from the other arms of the mesh via the coupler. This branch is fully accessible unless two links are broken, thus the probability that the arm is intact is:

$$P_{\text{arm}} = \left(1 + \sum_{t=1}^{\frac{n}{4}} \frac{1-p_t}{p_t}\right) \prod_{j=0}^{\frac{n}{4}} p_j = p_I p_L^{n/4} \tag{10}$$

and assuming all branches are identical then the probability that all 4 branches are intact is:

$$P_{\text{mesh}} = {P_{\text{arm}}}^4 \tag{11}$$

4. Numerical evaluation

The relative robustness of the different proposed topologies will be explored through numerical evaluate of the equations given above. The representative parameter values used are listed below:

Fibre length, $L = 1$ m

Fault probability per meter of fibre, $p = 1 \times 10^{-3}$

Fault probability at inlet port $1 \times 10^{-4} < P_I < 1 \times 10^{-1}$

Number of sensors, $n = 16$ or $n = 100$

Using these parameters the probability that all sensors are visible for interrogation are shown in Fig. 9 on **(a)** linear axes and **(b)** logarithmic axes. Fig. 10 shows the probability of a sensor being inaccessible, e.g. $1 - P_{\text{mesh}}$, on logarithmic axes.

As expected, increasing the probability of a fault in the inlet port increase the likelihood that sensors will be isolated. Considering the trends for each topology in turn:

4.1. Single ended line configuration

This has the lowest probability of survival across all probabilities of inlet port failure. At low inlet port failure probability, the failures are dominated by failures in individual fibre links where any single failure will result in sensors being isolated. As the probability of failure at the inlet port increases the overall probability of survival drops in proportion.

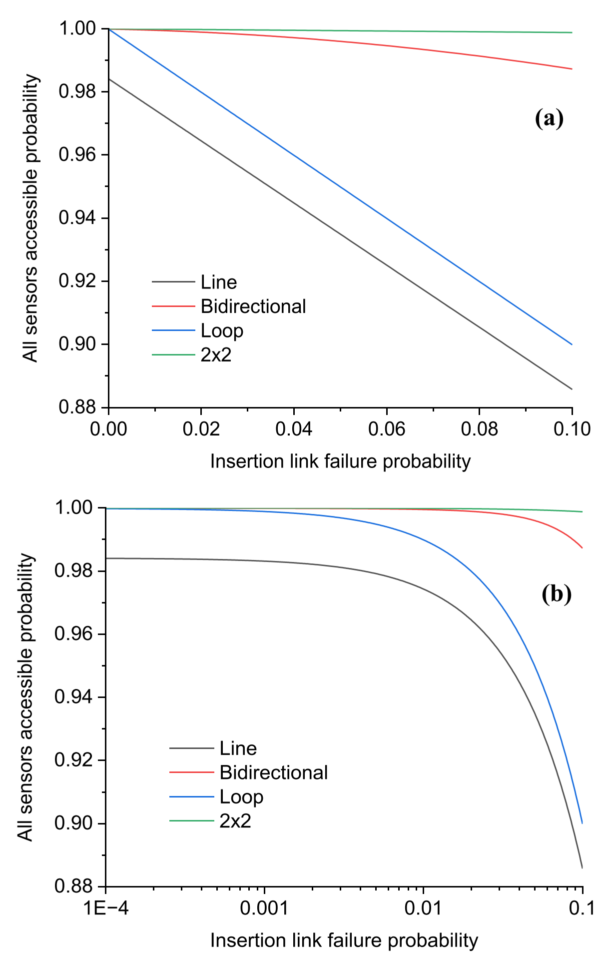

Fig. 9. Probability of all sensors being accessible for $n = 16$, $L = 1$ m, $p = 10^{-3}$ on **(a)** linear axes and **(b)** logarithmic axes.

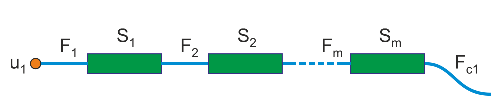

Fig. 8. Single arm of 2×2 mesh.

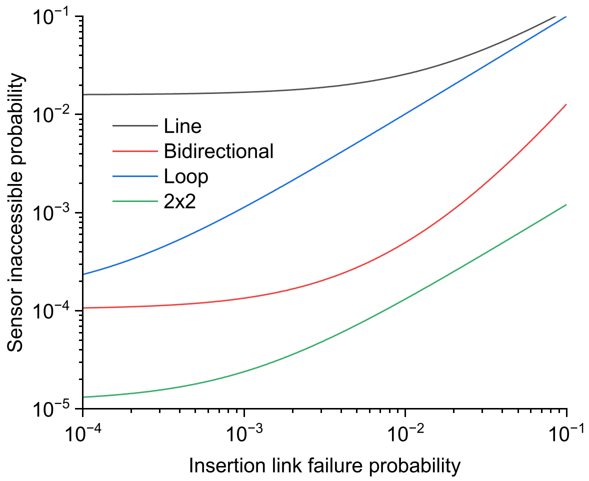

Fig. 10. Probability of any sensor being isolated for $n = 16$, $L = 1$ m, $p = 10^{-3}$.

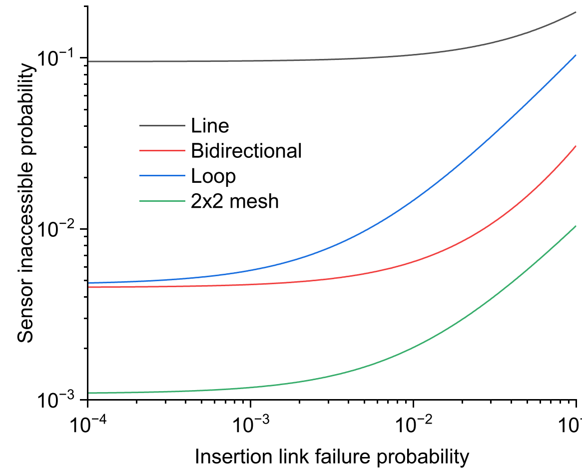

Fig. 11. Probability of any sensor being isolated for $n = 100$, $L = 1$ m, $p = 10^{-3}$.

4.2. Bidirectional line configuration and Dual Entry Loop configuration

The two inlet ports in these configurations provide redundancy in case one port is subject to failure and so this configuration provides good robustness for higher inlet port failure probability.

4.3. Single entry loop configuration

In this configuration the robustness behaviour is dominated by the inlet port fault probability (Fig. 9) since, once the optical signal is within the composite structure, the loop configuration means that sensors can be reached via two alternative routes and the effect of link faults is small. When the inlet port failure probability is below the link failure probability, the robustness is higher than the dual entry loop version since there are fewer links (Fig. 10).

4.4. 2×2 mesh configuration

The mesh configuration provides the greatest robustness of all of the configurations across all inlet port failure probabilities. This results from the several factors:

- each sensor can be interrogated from any one of 3 inlet ports so any two inlet port failures would not result in loss of a sensors;
- each arm of the mesh has $\frac{1}{4}$ of the number of links as in the other line/loop configurations so the probability of two failures within an arm is lower;
- each arm has an inlet port at one end and a coupler link at the other and so it is more robust than the bidirectional line configuration, which has inlet ports at each end.

If the number of sensors is increased (assuming the distance between sensors remains $L = 1$ m) then the probability of a link failure increases (comparing Fig. 10 and Fig. 11). This is particularly noticeable when the inlet link failure probability is low. However, the trends seen above remain, with the 2×2 mesh configuration giving significantly improved robustness with the probability of a sensor becoming isolated approximately 3 times lower than for the bidirectional line configuration and around two orders of magnitude lower than the simple line configuration.

5. Mesh interrogation

Having determined that the 2×2 mesh configuration offers greater robustness to damage than the other configurations considered, the question remains whether the individual sensor spectra can be disaggregated and the Bragg wavelengths determined with sufficient accuracy. This question must be addressed for both fault free and faulty conditions since, if the spectra cannot be disaggregated under fault conditions then the improved robustness does not provide any benefit. A further consideration is whether, in the 2×2 mesh, all of the sensors have distinct spectral features (e.g. Bragg wavelengths sufficiently separated that spectra do not substantially overlap under all stimulus conditions) or whether there is any overlap in their spectra. In the case of overlapping spectra, the disaggregation may be more challenging and the accuracy of Bragg wavelength estimation may be compromised. In the following sections, the case of non-overlapping spectra will be considered under no fault and fault conditions. Consideration of overlapping spectra will then be addressed.

5.1. Fault free conditions

In this initial analysis it will be assumed that each branch of the mesh contains a single sensor and that the spectra for all of the sensors are distinct. The extension to multiple sensors in each branch is trivial provided none of the sensors in any of the branches have overlapping spectra. In the simplified case, the mesh becomes that shown in Fig. 12.

It will also be assumed that the coupler provides a 50:50 split of the incoming optical signal to the two output fibres (coupling coefficient, $c = 0.5$), without any further losses or reflections. In this case, the reflected signal seen at input u_1 is made up of $R_1 = S_1 + \frac{1}{4}(S_2 + S_3)$, where the factor of $\frac{1}{4}$ arises because the light signal passes through the 50:50 coupler twice, once on the outward journey and once on the return.

In matrix form, the reflections at the four ports may be written as:

$$\begin{bmatrix} R_1 \\ R_2 \\ R_3 \\ R_4 \end{bmatrix} = \begin{bmatrix} 1 & \frac{1}{4} & \frac{1}{4} & 0 \\ \frac{1}{4} & 1 & 0 & \frac{1}{4} \\ \frac{1}{4} & 0 & 1 & \frac{1}{4} \\ 0 & \frac{1}{4} & \frac{1}{4} & 1 \end{bmatrix} \begin{bmatrix} S_1 \\ S_2 \\ S_3 \\ S_4 \end{bmatrix} = \frac{1}{4} \begin{bmatrix} 4 & 1 & 1 & 0 \\ 1 & 4 & 0 & 1 \\ 1 & 0 & 4 & 1 \\ 0 & 1 & 1 & 4 \end{bmatrix} \begin{bmatrix} S_1 \\ S_2 \\ S_3 \\ S_4 \end{bmatrix} \tag{12}$$

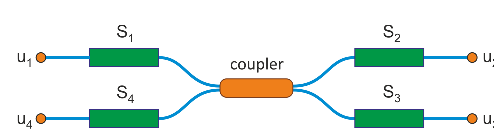

Fig. 12. Simplified mesh with a single sensor in each branch.

or

$$R = QS \tag{13}$$

Illustratively, assuming four spectra with Bragg wavelengths of 1, 2, 3 and 4 and reflection amplitude of unity, the individual spectra are as shown in Fig. 13 while the reflected signals at the four inputs are as shown in Fig. 14. In each case the amplitudes are offset by 1.1 units to aid clarity.

Inverting the matrix Q gives $\widehat{S} = Q^{-1}R$ and so we can estimate the individual sensor responses:

$$\begin{bmatrix} \widehat{S}_1 \\ \widehat{S}_2 \\ \widehat{S}_3 \\ \widehat{S}_4 \end{bmatrix} = \frac{1}{6}\begin{bmatrix} 7 & -2 & -2 & 1 \\ -2 & 7 & 1 & -2 \\ -2 & 1 & 7 & -2 \\ 1 & -2 & -2 & 7 \end{bmatrix}\begin{bmatrix} R_1 \\ R_2 \\ R_3 \\ R_4 \end{bmatrix} \tag{14}$$

The reconstructed spectra using this approach, with normally distributed noise of amplitude 0.1 units added to the reflected spectra, are shown in Fig. 15. As can be seen, the original spectra are largely recovered.

5.2. Faulty conditions

Under fault conditions, recovery of the individual FBG spectra using the method above may not be effective. Two fault conditions in different sections of the mesh may be considered as shown in Fig. 16.

The impact of these faults on the coupling matrix differs. In the case of Fault F_1, the reflected signals become:

$$\begin{bmatrix} R_1 \\ R_2 \\ R_3 \\ R_4 \end{bmatrix} = \begin{bmatrix} 0 & 0 & 0 & 0 \\ \frac{1}{4} & 1 & 0 & \frac{1}{4} \\ \frac{1}{4} & 0 & 1 & \frac{1}{4} \\ 0 & \frac{1}{4} & \frac{1}{4} & 1 \end{bmatrix}\begin{bmatrix} S_1 \\ S_2 \\ S_3 \\ S_4 \end{bmatrix} \tag{15}$$

or

$$R_{F1} = Q_{F1}S \tag{16}$$

If this fault is undetected and Fault-free recovery method is used, the resulting recovered spectra would be given by $\widehat{S} = Q^{-1}R_{F1}$. The result of this is shown in Fig. 17(a) for the illustrative system.

As may be seen, spectra for FBG 2–4 are recovered, although with

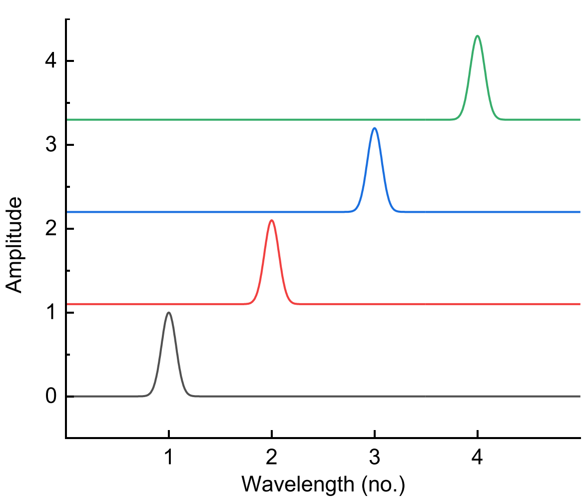

Fig. 13. Illustrative spectra for four Bragg gratings. Amplitudes are offset by 1.1 units each.

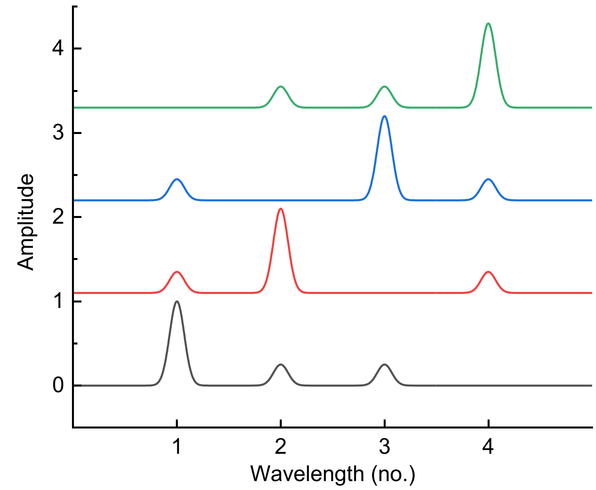

Fig. 14. Reflected spectra at each input.

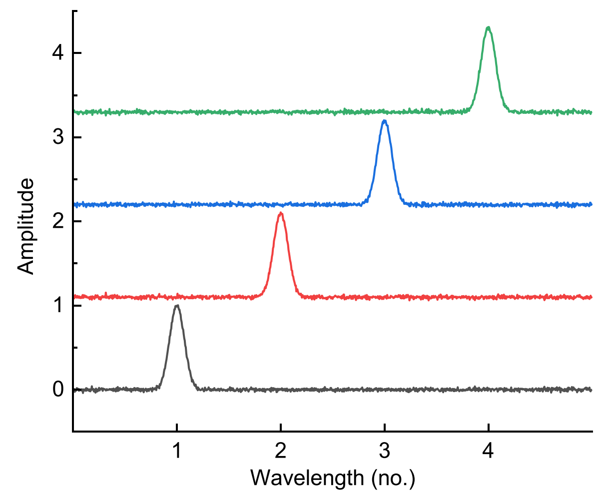

Fig. 15. Reconstructed FBG spectra.

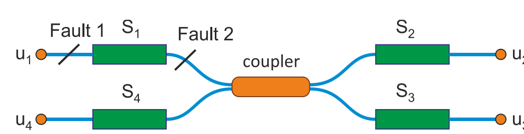

Fig. 16. Fault conditions considered.

different amplitudes than in the fault free case and with some additional spectra present at smaller amplitudes. The change in amplitude is unlikely to cause problems and, provided the expected Bragg wavelength range of each sensor is known, then the features outside of the expected range can be ignored. For FBG1, the expected spectral peak is not present on R_1. This observation could be used to detect the presence of Fault1 and an alternative method used to extract the Bragg wavelength.

Considering the structure of Q_{F1} it is not possible to invert this matrix. However, the lower right 3×3 submatrix may be inverted to reconstruct S_2, S_3, S_4. In addition, an estimate of S_1 may be extracted from R_2, R_3 or a combination of R_2 and R_3. Considering the first column of Q_{F1}, a logical option would be $\widehat{S}_1 = 2(R_2 + R_3)$, in which case the spectrum recovery equation becomes:

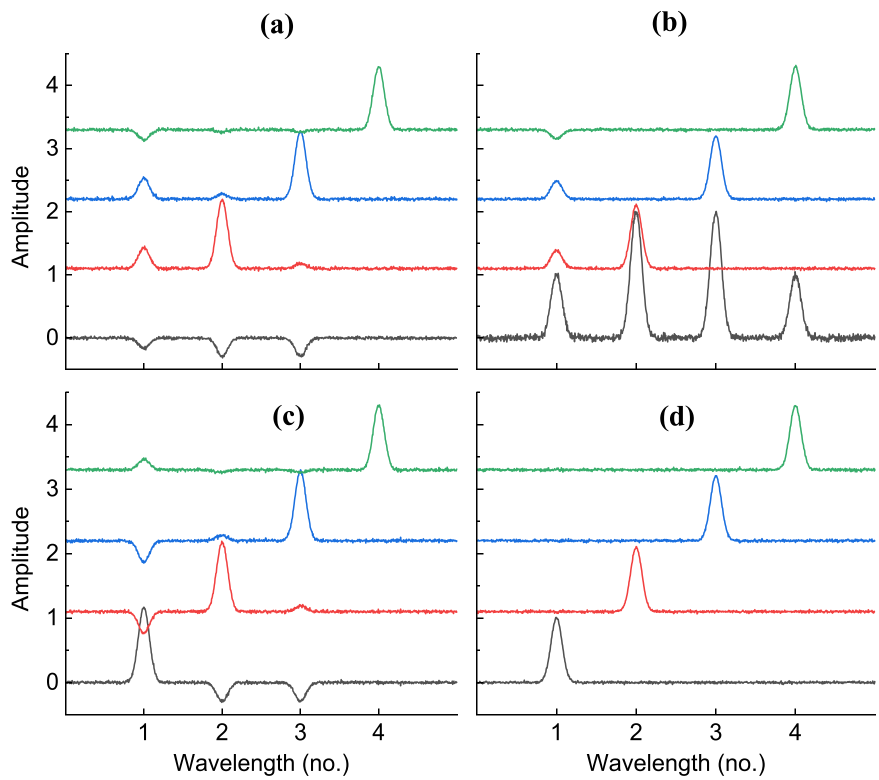

Fig. 17. Recovered spectra for **(a)** undetected Fault1, **(b)** known Fault1 with adapted spectrum recovery equation, **(c)** undetected Fault2, and **(d)** known Fault2.

$$\begin{bmatrix} \widehat{S}_1 \\ \widehat{S}_2 \\ \widehat{S}_3 \\ \widehat{S}_4 \end{bmatrix} = \frac{1}{14}\begin{bmatrix} 0 & 28 & 28 & 0 \\ 0 & 15 & 1 & -4 \\ 0 & 1 & 15 & -4 \\ 0 & -4 & -4 & 16 \end{bmatrix}\begin{bmatrix} R_1 \\ R_2 \\ R_3 \\ R_4 \end{bmatrix} \tag{17}$$

For the illustrative system the recovered spectra are presented in Fig. 17 (b). It can be seen that all peaks are present on the expected recovered signal but that there are large additional spectral peaks corresponding to other FBGs. If, however the wavelength range is limited to the anticipated range then these additional features will not interfere with Bragg wavelength estimation. It may also be noted from Fig. 17 (b) that the noise amplitude of recovered spectrum $\widehat{S}_1$ has larger amplitude than the other recovered spectra.

In the case of Fault2, the reflected signals become

$$\begin{bmatrix} R_1 \\ R_2 \\ R_3 \\ R_4 \end{bmatrix} = \begin{bmatrix} 1 & 0 & 0 & 0 \\ 0 & 1 & 0 & \frac{1}{4} \\ 0 & 0 & 1 & \frac{1}{4} \\ 0 & \frac{1}{4} & \frac{1}{4} & 1 \end{bmatrix}\begin{bmatrix} S_1 \\ S_2 \\ S_3 \\ S_4 \end{bmatrix} \tag{18}$$

or

$$R_{F2} = Q_{F2}S \tag{19}$$

If this fault is undetected and the Fault-free recovery method is used, the resulting recovered spectra would be given by $\widehat{S} = Q^{-1}R_{F2}$. The result of this is shown in Fig. 17 (c) for the illustrative system.

It can be seen that all of the expected peaks are present on the expected recovered signal, although with different amplitudes than in the fault free case and with some additional spectra present at smaller amplitudes. Once again, the change in amplitude is unlikely to cause problems and, provided the expected Bragg wavelength range of each sensor is known, then the features outside of the expected range can be ignored.

If the presence of Fault2 were detected, for instance by noting the peaks for S_2 and S_3 present in R_1, then this could be taken into account by inverting matrix Q_{F2}, giving

$$\begin{bmatrix} \widehat{S}_1 \\ \widehat{S}_2 \\ \widehat{S}_3 \\ \widehat{S}_4 \end{bmatrix} = \frac{1}{14}\begin{bmatrix} 14 & 0 & 0 & 0 \\ 0 & 15 & 1 & -4 \\ 0 & 1 & 15 & -4 \\ 0 & -4 & -4 & 16 \end{bmatrix}\begin{bmatrix} R_1 \\ R_2 \\ R_3 \\ R_4 \end{bmatrix} \tag{20}$$

Adopting this approach results in improved recovery of the individual spectra as shown in Fig. 17 (d).

6. Experimental evaluation

6.1. Experimental setup

A series of experiments were conducted to evaluate the 2×2 mesh network configuration. A small lab-scale interrogation setup, as presented in Fig. 1, was developed using an optical light source (DL-BP1–1501A, DenseLight Semiconductors), an interrogator system (I-MON 512, Ibsen Photonics), a 2×2 wideband fibre optic coupler (1550 ± 100 nm, 50:50 split, Thorlabs), and fibre Bragg grating sensors (FBGs). For the analysis of the 2×2 mesh configuration, each branch of the coupler was connected to a single FBG sensor (as shown in Fig. 12), and signals were interrogated in reflection mode. FBGs used for the experiments were purchased from Technica with centre wavelengths at 1550, 1552, 1555, and 1560 nm (± 0.5 nm), and their reflectivity and FWHM were ∼ 8–9% and ∼ 0.3 nm, respectively.

6.2. Results

Fig. 18 shows the spectrum with the four FBGs in a single daisy chain. Fig. 19 shows the four spectra obtained when the mesh is interrogated

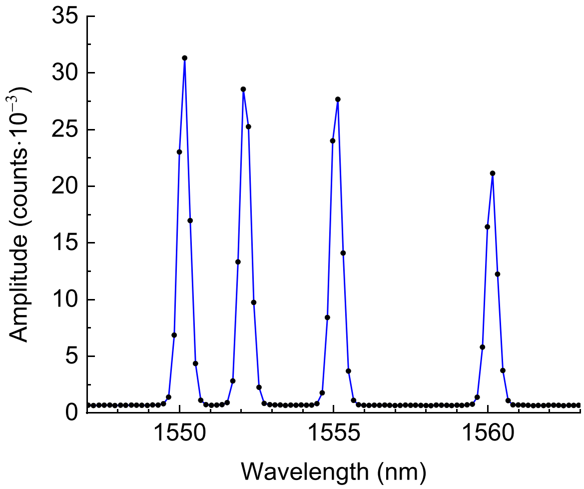

Fig. 18. Spectrum of daisy chained FBGs.

from each of the inputs respectively.

It may be seen that the expected spectral peaks are present in the individual reflected spectra but the amplitudes of the indirectly coupled peaks are significantly lower than ¼ of the main peak. It is believed that this is due to the coupling losses in various mating sleeves used to connect different components and sensors in addition to the light splitting in the coupler.

6.3. Spectral reconstruction

Assuming a perfect 50:50 coupler with no additional losses as above:

$$\begin{bmatrix} R_1 \\ R_2 \\ R_3 \\ R_4 \end{bmatrix} = \frac{1}{4}\begin{bmatrix} 4 & 1 & 1 & 0 \\ 1 & 4 & 0 & 1 \\ 1 & 0 & 4 & 1 \\ 0 & 1 & 1 & 4 \end{bmatrix}\begin{bmatrix} S_1 \\ S_2 \\ S_3 \\ S_4 \end{bmatrix} \tag{21}$$

and hence

$$\begin{bmatrix} \widehat{S}_1 \\ \widehat{S}_2 \\ \widehat{S}_3 \\ \widehat{S}_4 \end{bmatrix} = \frac{1}{6}\begin{bmatrix} 7 & -2 & -2 & 1 \\ -2 & 7 & 1 & -2 \\ -2 & 1 & 7 & -2 \\ 1 & -2 & -2 & 7 \end{bmatrix}\begin{bmatrix} R_1 \\ R_2 \\ R_3 \\ R_4 \end{bmatrix} \tag{22}$$

Results in the recovered spectra are shown in Fig. 20.

It can be seen in Fig. 20 that the main peaks are recovered but that there is significant residual from the other peaks. The coupling coefficient, c, may be adjusted in an attempt to take account of additional insertion losses. For instance, using $c = 0.3$ and adjusting the matrix coefficients in Eq. 21 accordingly, results in the reconstructed spectra shown in Fig. 21(a) where the reconstruction is improved, but not perfect. It appears that it is not possible to find a single value of c which entirely eliminates the subsidiary peaks in all cases.

An alternative approach is to estimate the coupling matrix from the individual spectra. Taking the peak amplitudes for each peak in the spectra shown in Fig. 19 and using these to populate the matrix:

$$Q_E = \begin{bmatrix} 31330028623729 \\ 03107034573581 \\ 25682882266400 \\ 37703232028540 \end{bmatrix} \tag{23}$$

In this case the reconstruction equation, $\widehat{S} = Q_E^{-1}R$ results in the spectra shown in Fig. 21 (b), where the normalised spectra are recovered and subsidiary peaks are almost entirely eliminated. An improved estimate of Q could probably be derived using a higher resolution spectra

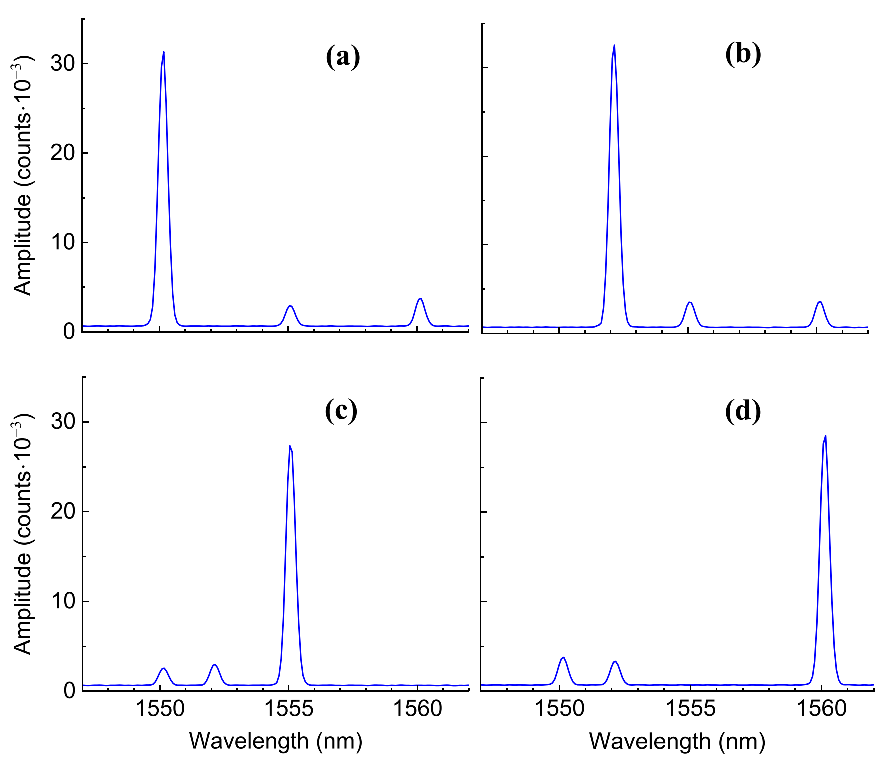

Fig. 19. Spectra of the structure measured from ports 1–4 (panels **(a)**–**(d)**).

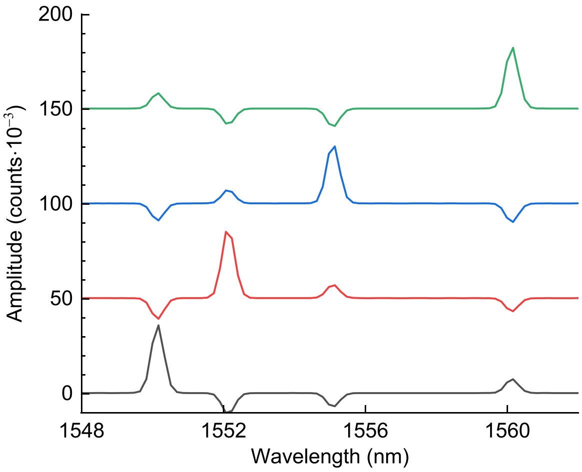

Fig. 20. Reconstructed spectra assuming coupling of 50%.

measured using an OSA or by fitting Gaussian functions to the spectra and extracting the peak amplitude from these.

6.4. Fault condition

In the presence of an undetected Fault1 the inversion of the full 4×4 matrix results in the reconstructed spectra shown in Fig. 22(a). As expected, the response of FBG1 is absent from channel 1 and a small signal is present in the other channels. The remaining peaks (FBG2–4) are present.

If fault F1 is detected and the same approach as above (invert the lower right 3×3 matrix and select a coefficient for elements1,2 and 1,3) results in inverse matrix

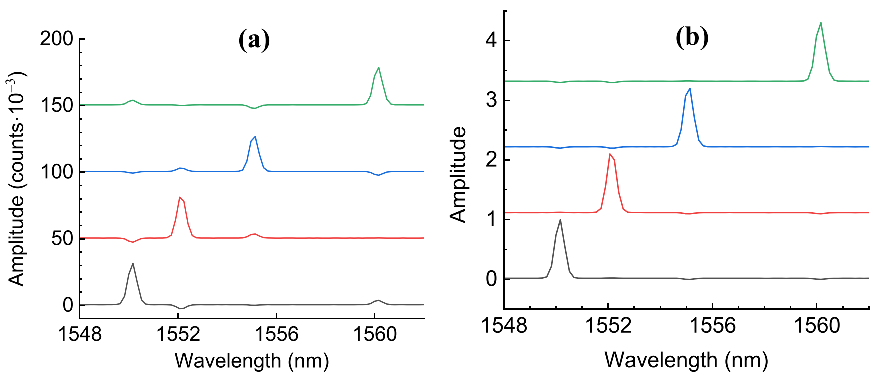

Fig. 21. Reconstructed spectra **(a)** with c = 0.3 and **(b)** using experimentally derived coupling matrix.

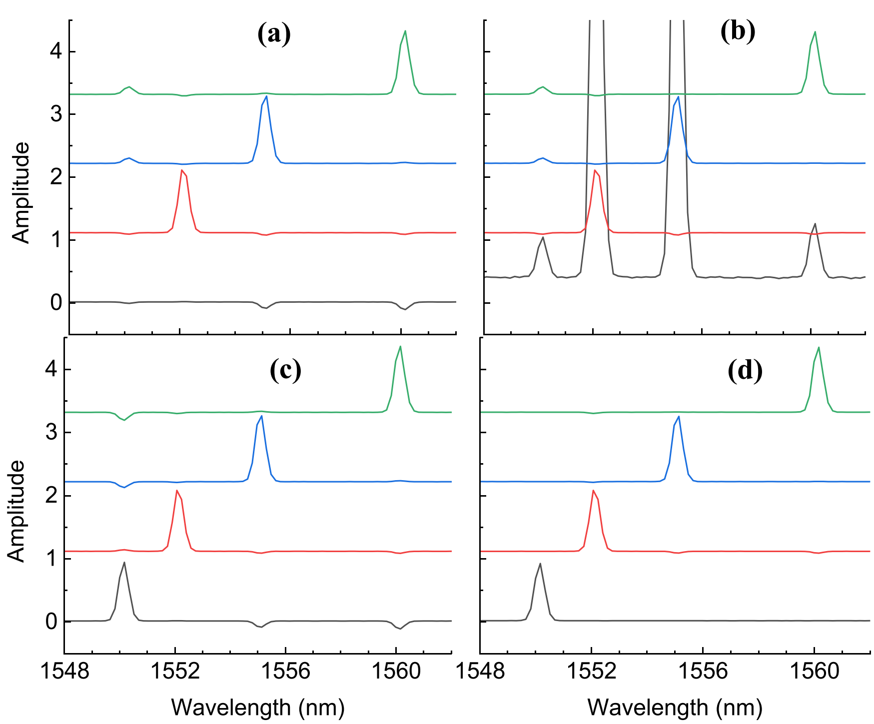

Fig. 22. Reconstructed spectra for **(a)** undetected Fault1, **(b)** detected Fault1, **(c)** undetected Fault2, and **(d)** detected Fault2.

$$Q^{-1} = 10^{-3}\begin{bmatrix} 0 & 0.3 & 0.3 & 0 \\ 0 & 0.0330 & -0.0043 & -0.0041 \\ 0 & -0.0036 & 0.0380 & 0.0004 \\ 0 & -0.0037 & 0.0005 & 0.0355 \end{bmatrix} \tag{24}$$

Giving the recovered spectra shown in Fig. 22 (b). It can be seen that the spectrum for FBG1 is present on channel one but large spurious peaks are present corresponding to FBGs 2–4.

In the case of an undetected Fault2, the reconstructed spectra are as shown in Fig. 22 (c). As can be seen, the spectrum for each FBG is present in the expected channel and spurious peaks are relatively small.

If Fault2 is detected and the appropriate terms in Q set to zero before inversion then the resulting recovered spectra are as shown in Fig. 22 (d), where it can be seen that all of the FBG peaks are present on the expected channels and the spurious peaks/troughs are small.

7. Conclusion

We have considered different mesh configurations of embedded fibre Bragg grating sensors with improved robustness for monitoring composite structures. The configurations of single ended line, bidirectional line, loop, and 2×2 mesh are analysed using a probabilistic model of sensor system robustness. The ability to interrogate a string or mesh of sensors from multiple inlet ports significantly improves robustness. Numerical evaluation of these configurations has shown that 2×2 mesh configuration provides the greatest robustness of all of the configurations across all inlet port failure probabilities. The probability of a sensor becoming isolated in the 2×2 mesh configuration is approximately 3 times lower than for the bidirectional line configuration. Using a matrix approach, the 2×2 mesh configuration is analysed in terms of disaggregation of individual sensor spectra for both fault free and faulty conditions. Simulation and experimental evaluation have demonstrated that successful recovery of individual grating spectra is possible with small spurious signals.

In this analysis it is assumed that the embedded couplers are immune to damage. The analysis may be extended to incorporate finite probability of coupler damage. In addition, it is assumed that all FBGs have a distinct Bragg wavelength and that reflection peaks do not overlap under the expected range of stimuli. If the FBGs peaks overlap in wavelength, it should not be a problem in the fault free case and even with faults it should be possible to reconstruct the original spectra if the matrix coefficients are known – but with some deterioration in signal-to-noise ratio. For a high number of sensors, an array of fibres may be adopted with optical switches used to interrogate each string successively. Further work is needed to explore the robustness if peaks do overlap under both fault free and fault conditions where the multiple optical paths provided by the mesh configuration may allow more successful disaggregation of peaks than is possible with the line or loop configurations.

While FBG are the most suitable for structural sensing, other types of optical fibre sensors can be studied for creating meshes with improved robustness, such as long-period fibre gratings, fibre interferometers, evanescent, etc. Such types of sensors have usually broader spectral features compared to FBGs, which reduces the number of sensors that can be multiplexed in wavelength. Time multiplexing is possible in this case; however, this would require different analysis regarding robustness of such systems. In case of FBG sensors, to optimize the number of sensors one needs first to choose the mesh structure in the sensing system. Then the number of FBGs, which is limited to typically around 10, depends on the optical bandwidth of light source and optical spectrum analyser, and the width of the spectral peak of single FBG.

The interrogation resolution of the sensor mesh depends on the accuracy of reconstruction of the grating spectra, which is determined by configuration of the optical scheme, noises in system and fault conditions. As we have shown in Sections 5 and 6, faults in the fibre mesh produce changes in amplitudes of the reconstructed signals with the spurious peaks at various wavelengths and also the noise amplitude of recovered spectrum increases. However, the spurious peaks are relatively small and the interrogation resolution would not be strongly affected by faults in the fibre mesh. In addition, various techniques for estimating the Bragg wavelength could be adopted to improve accuracy [23].

Funding

This work was supported by UK EPSRC under grants EP/W025108/1, EP/S000747/1 and EP/R004900/1.

CRediT authorship contribution statement

Oleg V. Ivanov: Writing – review & editing. **James M. Gilbert:** Conceptualization, Funding acquisition, Investigation, Supervision, Writing – original draft. **Kaushal Bhavsar:** Investigation, Software, Validation, Writing – review & editing.

Declaration of Competing Interest

The authors declare that they have no known competing financial interests or personal relationships that could have appeared to influence the work reported in this paper.

Data Availability

Data will be made available on request.

Acknowledgements

The authors acknowledge the contribution of Dr Tom Alsop in suggesting the adoption of the mesh configuration of sensors to improve robustness.

References

[1] L. Glavind, I.S. Olesen, B.F. Skipper, M.V. Kristensen, Opt. Eng. (2013), https://doi.org/10.1117/1.OE.52.3.030901.
[2] Zh Jiang, B. Wen, X. Tian, Z. Li, X. Dong, Z. Peng, Mar. Struct. (2020), https://doi.org/10.1016/j.marstruc.2020.102729.
[3] C. Marques, A. Leal-Júnior, S. Kumar, Materials (2023), https://doi.org/10.3390/ma16041433.
[4] R. Di Sante, Sensors (2015), https://doi.org/10.3390/s150818666.
[5] A. Güemes, A. Fernández-López, P.F. Díaz-Maroto, A. Lozano, J. Sierra-Perez, Sensors (2018), https://doi.org/10.3390/s18041094.
[6] R. Kashyap. Fiber Bragg Gratings, 2nd Edition, Academic Press, 2009, p. 632.
[7] M. Gotten, S. Lochmann, A. Ahrens, C. Benavente-Peces, 9th International Conference on Sensor Networks (2020), 23-28, https://doi.org/10.5220/0008942900230028.
[8] R.A.P. Herrera, M.F. Vallejo, M.L. Amo, Photon. Sens. (2012), https://doi.org/10.1007/s13320-012-0083-2.
[9] C. Chen, M. Sang, C. Ge, G. Chen, T. Liu, Proc. SPIE: International Conference on Optical Instruments and Technology: Optical Sensors and Applications (2015), https://doi.org/10.1117/12.2193411.
[10] X. Shibo, L. Tiegen, Z. Hongxia, G. Chunfeng, C. Cheng, D. Yang, J. Dagong, IEEE Sens. J. (2016), https://doi.org/10.1109/JSEN.2015.2472562.
[11] X. Song, Vacuum Assisted Resin Transfer Molding (VARTM): Model Development and Verification, Blacksburg (2003).
[12] P. Wei, X. Sun, A novel FBG sensor network with high survivability, Proc. SPIE: -Gener. Commun. Sens. Netw. (2006), https://doi.org/10.1117/12.685908.
[13] C.Y. Wu, K.M. Feng, P.C. Peng, C.Y. Lin, IEEE Photonics Technol. Lett. (2010), https://doi.org/10.1109/LPT.2010.2042709.
[14] Y. Zhang, J. Xin, Sensors (2019), https://doi.org/10.3390/s19214790.
[15] S.T. Hayle, Y.C. Manie, A.M. Dehnaw, Y.-T. Hsu, J.-W. Li, H.-C. Liang, P.-C. Peng, Opt. Commun. (2021), https://doi.org/10.1016/j.optcom.2021.127286.
[16] P. Urquhart, H. Palezi, P. Jardin, J. Light. Technol. (2011), https://doi.org/10.1109/JLT.2011.2129553.
[17] C.H. Yeh, N. Tsai, Y.H. Zhuang, C.W. Chow, W.F. Liu, IEEE Sens. J. (2016), https://doi.org/10.1109/JSEN.2016.2609458.
[18] H. Zhang, S. Wang, Y. Gong, T. Liu, T. Xu, D. Jia, Y. Zhang, J. Light. Technol. (2013), https://doi.org/10.1109/JLT.2013.2246769.

[19] H. Zhang, Y. Gong, D. Jia, T. Liu, Y. Zhang, IEEE Sens. J. (2015), https://doi.org/10.1109/JSEN.2014.2362915.
[20] A.M. Gillooly, L. Zhang, I. Bennion, Proc. SPIE: Photonics North (2004), https://doi.org/10.1117/12.567415.
[21] D. Jia, J. Chen, Y. Yan, H. Zhang, T. Liu, Y. Zhang, Opt. Fiber Technol. (2017), https://doi.org/10.1016/j.yofte.2017.09.013.
[22] D. Jia, Y. Zhang, Z. Chen, H. Zhang, T. Liu, Y. Zhang, IEEE Photonics J. (2015), https://doi.org/10.1109/JPHOT.2015.2442175.
[23] D. Tosi, Sensors (2017), https://doi.org/10.3390/s17102368.

James Gilbert is Professor of Engineering at the University of Hull. He completed Bachelor of Engineering (1986) and PhD (1989) degrees at the University of Hull. Since then he has held Lecturer, Senior Lecturer and Professor positions, also at the University of Hull. His research has focussed on instrumentation and measurements systems in a wide range of sectors including robotics, medical, manufacturing and energy. His current research focus is on manufacturing and performance monitoring in the offshore renewable energy sector, with a particular focus on composite structures in offshore wind energy. He is a Chartered Engineer and a Member of the Institution of Engineering and Technology.

Kaushal Bhavsar is Postdoctoral Researcher in Offshore Renewable Energy at the University of Hull. He obtained his PhD in Engineering from The Robert Gordon University in 2016 and MSc in Nanotechnology and Nanoelectronic Devices from the University of Surrey in 2011. He has a BEng degree in Electronics and Communication from the Hemchandracharya North Gujarat University in India. His research involved the development of fibre optic sensors, surface plasmon resonance sensors, and synthesis of metal/metal oxide nanomaterials for application in environmental sensing and monitoring, medical technology and offshore renewable energy systems. Currently, his work is mainly focused on the development of fibre optic sensing systems for offshore renewable energy structures.

Oleg V. Ivanov received the M.Sc. degree in physics and engineering from the Branch of Moscow State University in Ulyanovsk, Russia, in 1995. He received the Ph.D. degree in physical-mathematical sciences at the Ulyanovsk State University, Russia, in 1998. Since then he worked at this university until 2001 as Assistant Professor of the Department of Quantum Electronics and Optoelectronics of Physical Faculty. From 2001 until 2003, he was with the Department of Electrical Engineering, National Taiwan University. Then he was a Researcher at the Ulyanovsk Branch of Institute of Radio Engineering and Electronics of Russian Academy of Sciences until 2023. For two years (2005–2007), he was a Senior Researcher at the Optoelectronics and Electronics Unit of INESC Porto, Portugal. He is currently working on the investigation of fiber cladding modes, long-period fiber gratings, and fiber sensing at the University of Hull.